Wind and Structures, *Vol. 23, No. 6 (2016) 505-521*
DOI: http://dx.doi.org/10.12989/was.2016.23.6.505

Computational analysis of pollutant dispersion in urban street canyons with tree planting influenced by building roof shapes

Lakhdar Bouarbi*, Bouabdellah Abed[a] and Mohamed Bouzit[b]

Laboratoire de mécanique appliquée, Faculté de génie mécanique, Université des sciences et de la technologie d'Oran – Mohamed-Boudiaf, BP 1505, Oran El M'Naouer, 31000, Oran, Algeria

(Received November 27, 2015, Revised September 8, 2016, Accepted September 12, 2016)

Abstract. The objective of this study is to investigate numerically the effect of building roof shaps on wind flow and pollutant dispersion in a street canyon with one row of trees of pore volume, P_{vol} = 96%. A three-dimensional computational fluid dynamics (CFD) model is used to evaluate air flow and pollutant dispersion within an urban street canyon using Reynolds-averaged Navier–Stokes (RANS) equations and the Explicit Algebraic Reynolds Stress Models (EARSM) based on k-ε turbulence model to close the equation system. The numerical model is performed with ANSYS-CFX code. Vehicle emissions were simulated as double line sources along the street. The numerical model was validated by the wind tunnel experiment results. Having established this, the wind flow and pollutant dispersion in urban street canyons (with six roof shapes buildings) are simulated. The numerical simulation results agree reasonably with the wind tunnel data. The results obtained in this work, indicate that the flow in 3D domain is more complicated; this complexity is increased with the presence of trees and variability of the roof shapes. The results also indicated that the largest pollutant concentration level for two walls (leeward and windward wall) is observed with the upwind wedge-shaped roof. But the smallest pollutant concentration level is observed with the dome roof-shaped.

Keywords: street canyon; pollutant dispersion; trees; building configuration; numerical simulation; EARSM

1. Introduction

In cities across the globe, the traffic emissions are a major source of air pollution especially in downtown streets. This air pollution can have adverse effects on humans and the ecosystem. For this reasons, the air quality inside the urban street canyons is mainly controlled by canyon geometry and meteorological conditions. Quite a number of experimental and numerical studies have been carried out to investigate the urban air quality problems, the flow and transport mechanism in street canyons (Baik and Kim 1999, Chang and Meroney 2003, Di Sabatino, Buccolieri *et al.* 2008, Eliasson, Offerle *et al.* 2006, Gerdes and Olivari 1999, Hanna, Tehranian *et al.* 2002, Kastner-Klein and Plate 1999, Kastner-Klein, Fedorovich *et al.* 2001, Meroney,

*Corresponding author, Ph.D., E-mail: lakhdar.bouarbi@univ-usto.dz
[a] Ph.D., E-mail: ba_abed@yahoo.fr
[b] Professor, E-mail: bouzit_mohamed@yahoo.fr

http://www.techno-press.org/?journal=was&subpage=8 ISSN: 1226-6116 (Print), 1598-6225 (Online)

Pavageau *et al.* 1996, Meroney, Leitl *et al.* 1999, Pavageau and Schatzmann 1999). These studies deal with prevailing atmospheric wind directed perpendicular to the street axis.

Several numerical simulations, using computational fluid dynamics models, have been done fur prediction of flow and dispersion within street canyons. Sini, Anquetin *et al.* (1996) have used a standard k-ε model to show that the heating of street canyon surfaces would significantly affect fluid flow and pollutant transport. Kim and Baik (2001), Sahm, Louka *et al.* (2002) have evaluated the pollutant concentration in different isolated two-dimensional urban street canyons using the standard $k-\varepsilon$ turbulence models. Chan, Dong *et al.* (2002) have also applied the three versions of the k-ε turbulence model on a two-dimensional street canyon and concluded that the RNG k-ε turbulence model was found to be the optimum. Nazridoust and Ahmadi (2006) simulated using the FLUENT code, the dispersion of gaseous and particles exhaust emissions in different street canyons. Cai, Barlow *et al.* (2008) applied a large-eddy simulation (LES) model to a street canyon in order to derive the fields of wind, turbulence, scalar concentration, concentration fluctuations, and scalar flux across the roof level. Santiago and Martín (2008) investigated the pollutant dispersion inside a street canyon using SLP-2D (street Lagrangian particles).

In the recent years, the influence of presence trees planting in a street canyon on air quality has gained more importance. Gromke and Ruck (2007, 2009) performed wind tunnel experiments on the influence of tree planting patterns on the natural ventilation and pollutant dispersion within a street canyon. They found that trees planting increase the traffic-induced pollutant concentrations inside the street canyon when compared to the treeless case. Gromke, Buccolieri *et al.* (2008) and Buccolieri *et al.* (2009) examined the influence of avenue-like tree planting on flow and traffic exhaust dispersion in urban street canyons with different crown porosity in a typical street canyon using CFD and wind tunnel models. The results indicated that the vegetation reduces ventilation, which lead to high pollutant concentration local wise. The impact of avenues of trees on traffic pollutant dispersion and concentrations in urban street canyons, with different tree-avenue models in combination with variations in street-canyon approaching wind direction, was numerically and experimentally investigated by Buccolieri, Salim *et al.* (2011) and Gromke and Ruck (2012). They concluded that the prevailing assumption that attributes the most harmful dispersion conditions to a perpendicular wind direction does not hold for street canyons with avenues of trees. Salim, Riccardo *et al.* (2011), Moonen, Gromke *et al.* (2013) applied a large-eddy simulation (LES) model to a street canyon with and without trees. It was concluded that LES is capable to quantitatively predict pollutant dispersion. Recently, Gromke and Blocken (2015a, b) studied the flow and dispersion of traffic-emitted pollutant in a generic urban neighborhood with multiple layouts of avenue-trees using Reynolds-averaged Navier Stokes equations (RANS) with realizable k-ε turbulence closure. They concluded that the qualitative and not only quantitative changes in the flow field were observed at the neighborhood wise when compared to the avenue-like tree planting at the street canyon wise.

The impact of roof shapes on the flow and pollutant dispersion characteristics in street canyon has been studied over the past few decades to help understand the flow pattern and pollutant transport inside urban street canyons. Xie, Huang *et al.* (2005) employed CFD techniques for the analysis of the effect of different roof shapes and nearby buildings structures on the mean flow field inside an urban canyon. Huang, Hu *et al.* (2009) provided numerical simulations of airflow and pollutant dispersion within urban street canyons of different wedge-shaped roof combinations and reveal the impact of wedge-shaped roofs on in canyon wind flow and pollutant distribution patterns. These studies indicated that there is an important influence of the roof shapes on the wind field and the pollutant dispersion in the street canyon. All of these studies were carried out in bi-dimensional domain.

The present work presents three-dimensional CFD simulations; the aim is to analysis the impact of building roof shapes on flow and pollutant dispersion in urban street canyons with one row of trees, in order to find the optimal roof shape that would enhance ventilation. Vehicle emissions were simulated as double line sources along the street. Numerical results were validated using an extensive wind-tunnel (WT) experimental database, which were carried out at the University of Karlsruhe, Germany, and were assessable to the scientific community from the online database (2008).

2. Methodology

2.1 Numerical model

Pollutant dispersion in urban street canyons is usually investigated numerically using a two or three-dimensional model. In this study, the Explicit Algebraic Reynolds Stress Models EARSM (Wallin and Johansson 2000) within the steady state Reynolds Averaged Navier-Stokes (RANS) framework was used to simulate the flow field and pollutant dispersion in street canyons with various building roof shape configurations. This model is based on two equations *k*-*ε* turbulence model with the nonlinear eddy viscosity model and explicit terms for anisotropic parts of the Reynolds stress tensor with computational requirements similar to the standard *k*-*ε* model.

The EARSM enables an extension of the current *k*-*ε* turbulence models to capture the flow effects such as the secondary flow flied with streamline curvature and system rotation (ANSYS CFX 2013).

The turbulent kinetic energy, $k = \overline{u_i u_i}/2$, and its dissipation, ε, are determined from the transport equations

$$\frac{Dk}{Dt} + \frac{\partial T_l^{(k)}}{\partial x_i} = P_k - \varepsilon \tag{1}$$

$$\frac{D\varepsilon}{Dt} + \frac{\partial T_l^{(\varepsilon)}}{\partial x_i} = \left(C_{\varepsilon 1} P_k - C_{\varepsilon 2} f\, \varepsilon\right)\frac{\varepsilon}{k} \tag{2}$$

The transport terms, $T_l^{(k)}$ and $T_l^{(\varepsilon)}$ applied to the turbulent kinetic energy and its dissipation give

$$T_l^{(k)} = -c_s' \frac{k}{\varepsilon}\overline{u_l u_m}\frac{\partial k}{\partial x_m}, \quad T_l^{(\varepsilon)} = -c_\varepsilon \frac{k}{\varepsilon}\overline{u_l u_m}\frac{\partial \varepsilon}{\partial x_m} \tag{3}$$

where $c_s' = 0.25$, $c_\varepsilon = 0.15$, $c_\mu = 0.09$, $c_{1\varepsilon} = 1.44$, $c_{2\varepsilon} = 1.92$ are constants determined experimentally from a wide range of turbulent flows and P_k is the turbulence production.

With EARSM, the Reynolds stresses are computed from the anisotropy tensor according to its definition

$$\overline{u_i u_j} = k\left(a_{ij} + \frac{2}{3}\delta_{ij}\right) \tag{4}$$

The anisotropy tensor a_{ij} is expressed as a polynomial based on the strain rate and the vorticity tensors as follows

$$\begin{aligned} a_{ij} &= \beta_1 S_{ij} + \beta_3\left(\mathbf{\Omega}_{ik}\mathbf{\Omega}_{kj} - \frac{1}{3} II_{\mathbf{\Omega}}\delta_{ij}\right) + \beta_4\left(S_{ik}\mathbf{\Omega}_{kj} - \mathbf{\Omega}_{ik}S_{kj}\right) \\ &+ \beta_6\left(S_{ik}\mathbf{\Omega}_{kl}\mathbf{\Omega}_{lj} + \mathbf{\Omega}_{ik}\mathbf{\Omega}_{kl}S_{lj}\right) + \beta_9\left(\mathbf{\Omega}_{ik}S_{kl}\mathbf{\Omega}_{lm}\mathbf{\Omega}_{mj} - \mathbf{\Omega}_{ik}\mathbf{\Omega}_{kl}S_{lm}\mathbf{\Omega}_{lj}\right) \end{aligned} \tag{5}$$

S_{ij} and Ω_{ij} are the non-dimensional strain-rate and vorticity tensors, respectively. They are defined as

$$S_{ij} = \frac{1}{2}\tau\left(\frac{\partial U_i}{\partial x_j} + \frac{\partial U_j}{\partial x_i}\right) - \frac{1}{3}\delta_{ij}\tau\frac{\partial U_k}{\partial x_k} \tag{6}$$

$$\mathbf{\Omega}_{ij} = \frac{1}{2}\tau\left(\frac{\partial U_i}{\partial x_j} - \frac{\partial U_j}{\partial x_i}\right) + \tau\,\mathbf{\Omega}_k^{rot} \tag{7}$$

where $\mathbf{\Omega}_k^{rot}$ is the components of the coordinate system rotation vector and τ is the turbulent time scale defined as

$$\tau = \max\left(\frac{k}{\varepsilon}, 6.0\sqrt{\frac{\nu}{\varepsilon}}\right). \tag{8}$$

The β -coefficients are equal to

$$\left.\begin{aligned} &\beta_1 = -\frac{N\left(2N^2 - 7II_{\mathbf{\Omega}}\right)}{Q}, \quad \beta_3 = -\frac{12\,N^{-1}IV}{Q}, \\ &\beta_4 = -\frac{2\left(N^2 - 2II_{\mathbf{\Omega}}\right)}{Q}, \quad \beta_6 = \frac{-6\,N}{Q}, \ \beta_9 = \frac{6}{Q} \end{aligned}\right\} \tag{9}$$

where

$$Q = \frac{5}{6}\left(N^2 - 2\,II_{\mathbf{\Omega}}\right)\left(2N^2 - II_{\mathbf{\Omega}}\right) \tag{10}$$

The invariants, which appear in the formulation of the anisotropy tensor and the coefficients, are defined by

$$II_{\mathbf{\Omega}} = \mathbf{\Omega}_{kl}\mathbf{\Omega}_{lk} \tag{11}$$

$$IV = S_{kl}\,\mathbf{\Omega}_{lm}\mathbf{\Omega}_{mk} \tag{12}$$

For more details see Wallin and Johansson (2000).

For dispersion calculations, the convection–diffusion equation was used. In turbulent flows it is given by

$$\nabla\cdot(\rho U\,\varphi)=\nabla\cdot\left(\left(\rho\,D_{\phi}+\frac{\mu_t}{Sc_t}\right)\nabla\varphi\right) \tag{13}$$

where U is the fluid velocity in the case of a fluid or porous domain, $\varphi = \phi/\rho$ is the conserved quantity per unit mass, ϕ is the conserved quantity per unit volume, or concentration , ρ is the mixture density, $D\phi$ is the kinematic diffusivity for the scalar, and $S_{ct} = 0.7$ is the turbulent Schmidt number.

The tree crowns are modeled as isotropic porous regions and assigned the pressure loss coefficient λ to the cells occupied by the crown. In ANSYS-CFX, the isotropic losses in porous regions model contributes a momentum sink to the standard fluid flow equations incorporates an empirically determined flow resistance in the region of the computational domain defined as porous. The momentum loss through an isotropic porous region can be formulated using permeability and loss coefficients as follows

$$S_{M,i}=-\frac{\mu}{K_{perm}}U_i-\lambda\frac{\rho}{2}|U|U_i \tag{14}$$

where $S_{M,i}$ is the source term for the i th (x, y, or z) momentum equation, $|U|$ is the magnitude of the velocity, λ is the pressure loss coefficient and K_{perm} is the permeability, this term can be calculated as

$$K_{perm}=\left(\left(D_p^2\right)e^3\right)/\left(150\left(1-e\right)^2\right) \tag{15}$$

where e = 0.96 is the porosity (void fraction) and D_p = 6 (Volume of Particle/Surface Area of Particle) is the equivalent spherical diameter of particle.

The linear component of this source represents viscous losses and the quadratic term represents inertial losses. The source may alternatively be formulated using linear and quadratic resistance coefficients, substituting two coefficients C_{R1} and C_{R2} as follows

$$C_{R1}=\frac{\mu}{K_{perm}} \tag{16}$$

$$C_{R2}=\lambda\frac{\rho}{2} \tag{17}$$

2.2 Model domain and grids

Fig. 1 shows the isolated street canyon configurations with tree planting. We consider six different configurations of roof shapes of buildings forming the street canyon containing the line sources (S) and can be divided into respectively: the flat roof-shaped (case 1), upwind wedge roof-shaped (case 2), downwind wedge roof-shaped (case 3), slanted roof-shaped (case 4), dome roof-shaped (case 5) and trapezoidal roof-shaped (case 6). The roof height for cases 2, 3, 4, 5 and 6 is $H/3$ with H being the building height. The line sources of pollutant (Sulfur hexafluoride (SF_6)) with constant emission rate are placed at the test canyon floor to model the emission source from the vehicular exhaust. The wind is orthogonal to the direction of the street. All urban street canyons have the following dimensions: the height of the building H = 120 mm, the width of the building B = 120 mm and the width of the street W = 120 mm. The free stream velocity $U(Z_{ref} = H)$ = 4.70 m/s. The trees were positioned horizontally centered in the street canyons with crowns of $H/2$ width and $2/3H$ height, starting $H/3$ above the street level (see Fig. 3(b)).

As illustrated in Fig. 2, a three-dimensional computational domain was used with the wind flow direction assumed to be perpendicular to the street canyon.

The computational domain was discretized using hexahedral elements (Fig. 3(a)). Extensive tests of the grid intervals are carried out with increasing grid interval until further refinement is shown to be less significant. The chosen grid is finer close to the building and ground, and then it expanded further away. A mesh with a total cell count of 1.09 million is selected. The grid intervals near the roof in the x- , y- and z-directions are $\Delta x = \Delta y = \Delta z = 0.1H$.

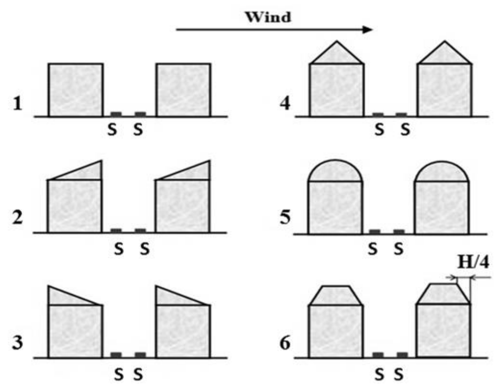

Fig. 1 Computational urban street canyon configurations

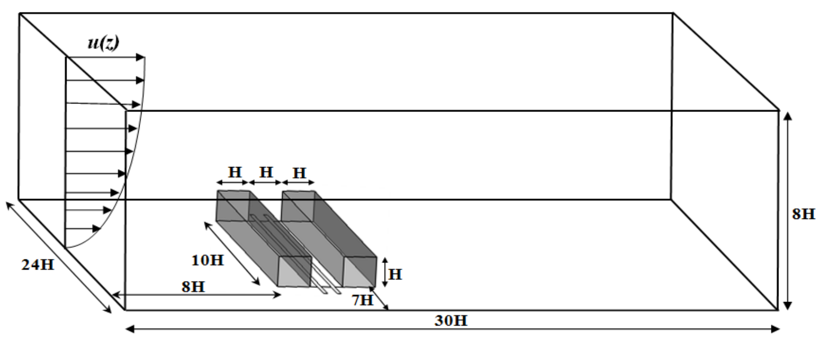

Fig. 2 Computational domain

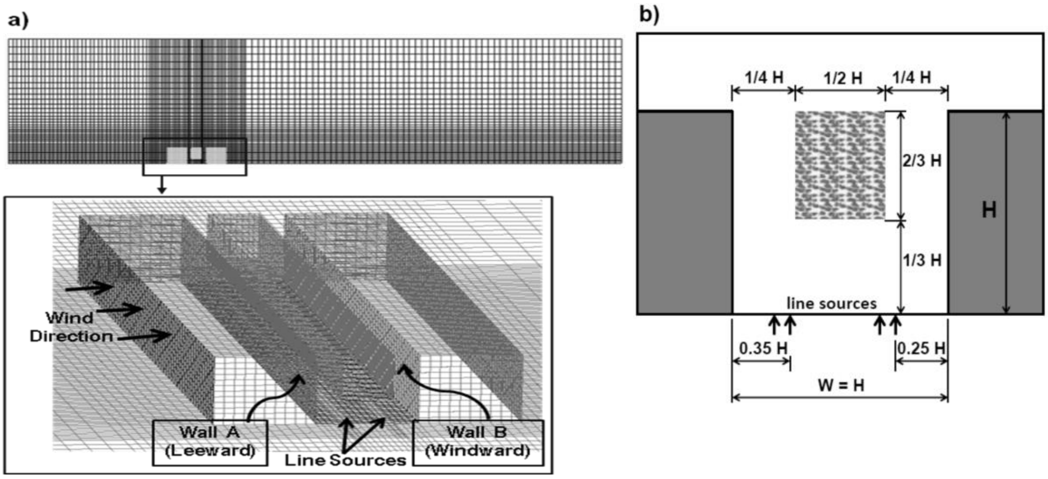

Fig. 3 (a) Computational grid of the domain (case 1) (ICEM-CFD) and (b) Sketch of the position of line sources and tree models dimensions

2.3 Boundary conditions

The boundary conditions set are the following: At inflow boundary, the profile of the horizontal velocity *u(z)*, the turbulent kinetic energy $k(z)$ and its rate of dissipation $\varepsilon(z)$ are specified, while the vertical and lateral wind velocity and the pollutant concentration are imposed to be zero. At the outflow boundary, the gradients with respect to the streamwise direction are set to zero. Symmetry conditions are specified for the top and lateral sides of the computational domain to enforce a parallel flow. Non-slip conditions are applied for the building walls and floors. The profile of the horizontal velocity *u(z)* is represented in the power law profile form as

$$u(z) = u(z_{ref})\left(\frac{z}{z_{ref}}\right)^{0.3} \tag{18}$$

The turbulent kinetic energy k and its rate of dissipation ε are specified at the inlet boundary conditions as

$$k(z) = \frac{u_*^2}{\sqrt{C_\mu}}\left(1 - \frac{z}{\delta}\right) \tag{19}$$

and

$$\varepsilon(z) = \frac{u_*^3}{\kappa z}\left(1 - \frac{z}{\delta}\right) \tag{20}$$

where δ is the boundary layer thickness (≈ 0.5 m), $u_* = 0.54$ m s^{-1} is the friction velocity (known from log-law curve fitting of WT mean velocity profile), κ is the von Kàrmàn constant (0.4) and $C\mu$ = 0.09. In ANSYS-CFX, the surface roughness is expressed in terms of a sand grain roughness Ks instead of the roughness length Z_0 as it is the case in most meteorological codes. To circumvent problems with a coarse grid resolution near the ground due to large sand grain roughness values Ks, we set $Ks = Z_0$ which was found to be Z_0 equal to 0.0033 m from the wind tunnel experiments.

2.4 Model validation

The CFD code ANSYS-CFX software was employed in this study. The 3D Reynolds-Averaged Navier-Stokes (RANS) equations and the continuity equation are solved using the finite volume method. Closure is obtained using the EARSM based k-ε model. The transport equations were discretized by the finite volume method with the second order scheme for all terms. Pressure-velocity coupling is taken care of by a fully coupled algorithm. Pressure interpolation is second order. The scaled residual criteria for all the flow properties were set at $1x10^{-5}$.

The experimental data used for validation of the present model were obtained from a wind tunnel experimentation has been carried out at the Laboratory of Building and Environmental Aerodynamics in Karlsruhe Institute of Technology (KIT). WT concentration data are accessible to the scientific community and can be found online at <www.codasc.de>. The experimental setup and results have also presented and detailed by Gromke and Ruck (2007, 2009).

The wind tunnel experiments model (scale 1:150) consist of two parallel aligned rows of houses forming an isolated street canyon of length L = 180 m and height W = 18 m with two flanking buildings of height H = 18 m and width B = 18 m. The wind was perpendicular to the street axis with mean velocity profile exponent α = 0.30 and turbulence intensity profile exponent α_1 = 0.36 according to the power law formation were reproduced

$$\frac{u(z)}{u(z_{ref})} = \left(\frac{z}{z_{ref}}\right)^{\alpha} \tag{21}$$

and

$$\frac{I_u(z)}{I_u(z_{ref})} = \left(\frac{z}{z_{ref}}\right)^{-\alpha_1} \tag{22}$$

where, $I_u(z_{ref})$ is the mean turbulence intensity at height H (CODASC 2008).

Integrated in the model street, four Sulfur hexafluoride (SF6) tracer gas emitting line sources (Fig. 3(b)) were used for simulating the release of traffic exhausts with emission rate Q = 10 g s^{-1}. In order to account for the traffic exhausts released on the sidewise street intersections, the line source exceeded the street canyon by approximately 10% on each side. The line source strength was monitored and controlled by a flow meter, ensuring a constant tracer gas supply during the measurements. Mean concentrations of the SF6 gas were measured at the canyon walls and normalized according to with c which is the measured concentration; u_H flow velocity at height H in the undisturbed approaching flow and Q/l is the tracer gas source strength per unit length. The tree crowns were modeled as porous media, with a pore volume, P_{vol} = 96 % corresponding to a pressure loss coefficient, λ = 200 m^{-1} obtained from measurements in forced convection conditions.

The measurements were taken from specific points on the walls of the upwind and downwind buildings of the street canyon.

$$C^{+} = \frac{c u_H H}{Q / l} \tag{23}$$

Fig. 4 shows the computed and measured normalized pollutant concentrations *C*+ at walls (A and B) in the street canyon respectively. A good agreement between the numerical model and the wind tunnel experiment is observed.

3. Results and discussions

3.1 Air flow fields

There are a number of studies on flow field around an isolated building in neutrally stable boundary layers (Ahmadi and Li 2000, Becker, Lienhart *et al*. 2002). These studies describe the characteristics of basic wind flow patterns around the buildings of various shapes and orientations. This section focused at the effect of different roof shapes on the flow characteristics in street canyon. Fig. 5 shows the streamlines in street canyon with flat roof-shaped (reference case) subjected to perpendicular approaching flow. Two fundamental vortex structures can be observed. These are the clockwise canyon vortex inside the street canyons between the buildings, and the secondary vortex (corner eddies) located at the two ends of the street canyon (Fig. 5). The canyon vortex generated in the street canyon (reference case) is driven by the atmospheric cross-flow above roof level. At ground level, the flow is directed opposite to the atmospheric wind direction (from wall B towards the leeward wall A) and after, the canyon vortex and helical recirculation moves upward and are partially entrained into the atmospheric cross-flow above roof level (Gromke and Ruck, 2009). The corners eddies transport air from the outside environment directly into the street canyon, were provide additional ventilation and lead to lower traffic pollutant concentrations at the street canyon ends.

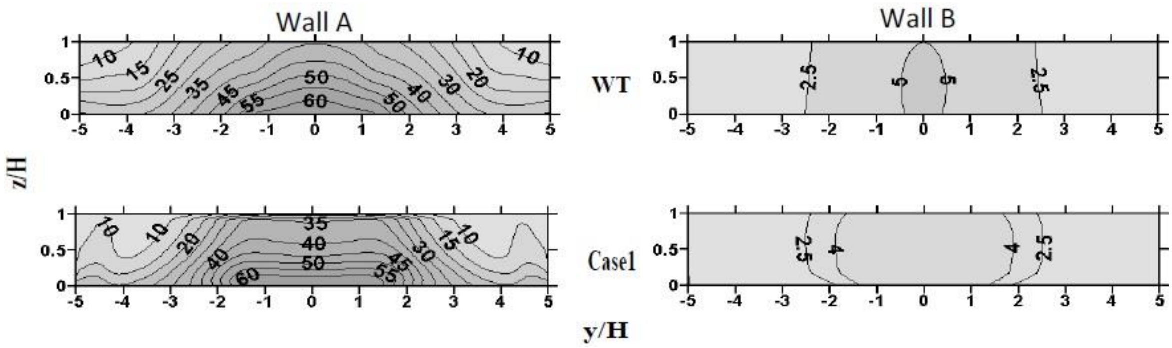

Fig. 4 Normalized pollutant concentrations C^{+} at walls (wall A and B) in the street canyon for wind tunnel data and numerical simulation (flat roof-shaped)

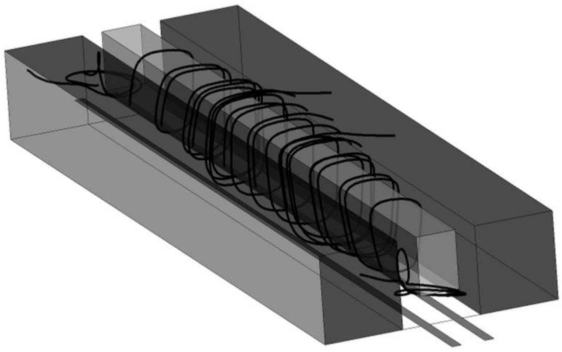

Fig. 5 Streamlines in street canyon with flat roof-shaped (reference case) obtained from CFD simulations

Fig. 6 shows the vectors and distribution of the vertical velocity at $y/H = 0$, inside the urban street canyons for six different roof configurations.

In case 1(flat-shaped roof), a large unique clockwise vortex can be found. The air flow near the trees is slow, and it becomes faster when it approaches the wall of the building and the ground level. However, a direct comparison reveals that the upward vertical velocities near wall A (leeward wall) are higher than the downward vertical velocities near wall B (windward wall). For case 2 (Upwind Wedge-shaped Roof), a couple of vortices with different directions are formed in the street canyons. Two clockwise vortexes are generated in the street canyon, one in the upper region and the other is formed around the trees. But a small counter-clockwise vortex is remarked upper of the street between the trees and downwind building. The upper vortex extends to the roof of the windward building. The highest vertical velocity is observed in the upper part of the street canyon near the upwind building roof while the lowest vertical velocity is near the right trees and the top of the downwind building roof.

The vortex circulation in case 3 (downwind wedge-shaped roof) appeared upwards in the upper region near the center street canyon, this vortex extends to the top of the upwind building roof. The lowest vertical velocity is observed near the wall B especially in the upper region nearby the roof of the upwind building of the street canyon. The highest vertical velocity appears near the wall A. In case 4 (slanted-shaped roof), a clockwise vortex appeared upwards in the upper region between the building roofs and it extends to the top of the upwind and downwind building roof, thus enhancing the air exchange between the outer flow and the canyon interior. The lowest vertical velocity is observed in the left side of the trees, while the highest vertical velocity appears in the upper region near wall A. In case 5 (dome roof-shaped), it can be seen clearly that the in- canyon air vertical velocity fields follow a similar pattern as the reference case (case 1). The highest vertical velocity is observed near wall A, while the lowest appears near wall B. In case 6 (trapezoid-shaped roof), it can be observed that the single clockwise vortex, with its center moving upward of the canyon and is finally located between the building roofs, thus enhancing the air exchange between the outer flow and the canyon interior. The lowest vertical velocity is seen near wall B and the downwind building roof of the street canyon, while, the highest vertical velocity appear near wall A.

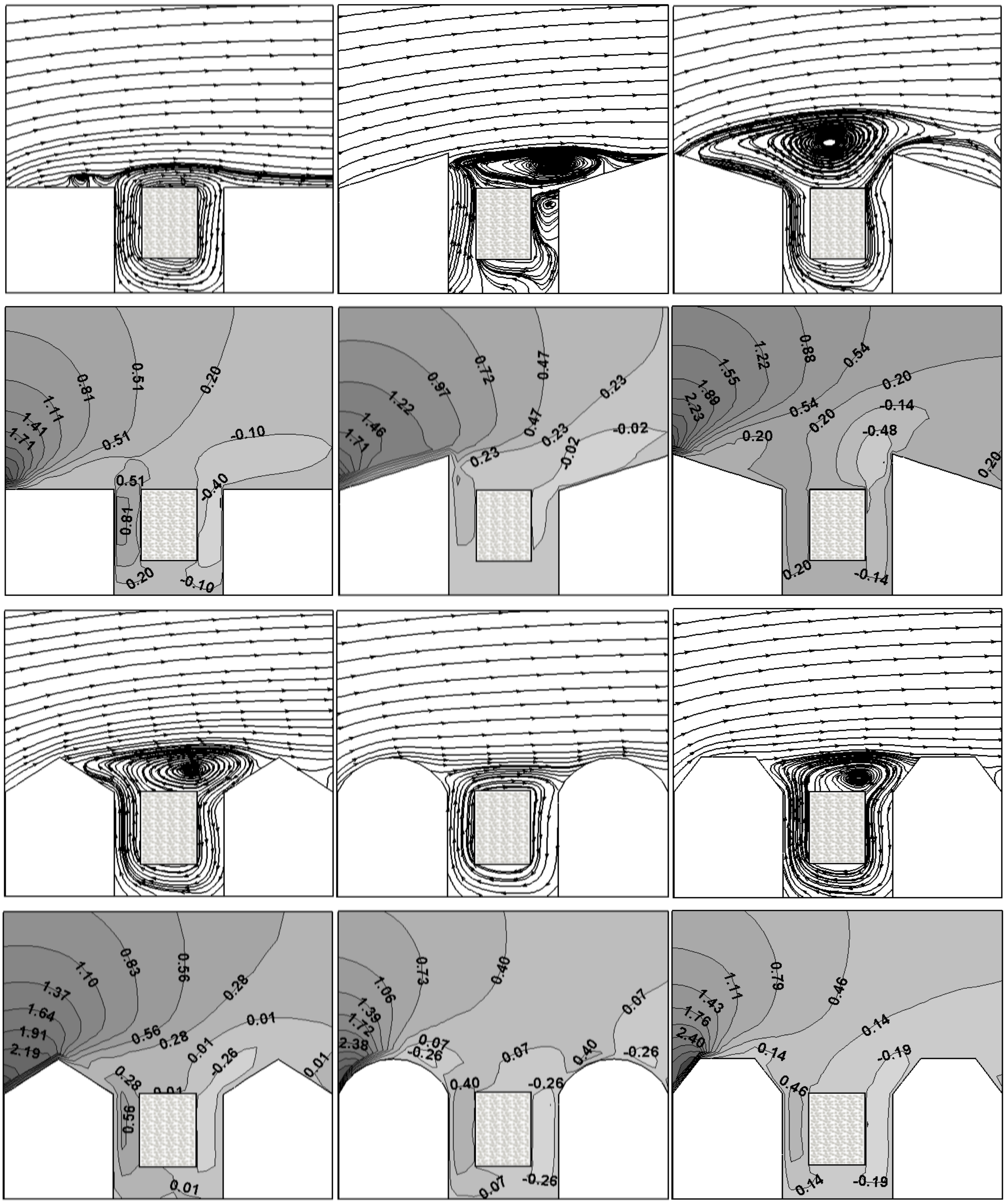

Fig. 6 Streamlines and distribution of the vertical velocity at the mid-plane *y/H*=0, inside the urban street canyons for six different roof configurations

3.2 Turbulent kinetic energy (TKE)

The distribution of turbulent kinetic energy (TKE) along the mid-plane of the street canyon at *y/H* = 0 for six different roof configurations are shown in Fig. 7. From these figures, a shear layer can be seen at the top of each canyon. However, the thickness of the shear layer changes with the change roof shapes. So the distribution of TKE is different for each canyon depending on the roof shapes and the position in a street canyon (*y/H*). The highest values of the TKE are found in the upper region toward the upwind building roof. This is due to the vigorous production of strong wind shear and also due to the advection of high TKE. But, the lowest turbulent kinetic energy was found at the points of separation and reattachment related to the corner of the upwind and downwind building downstream of the street canyon. The TKE is observed to be higher for downwind wedge-shaped (case 3) roof, dome roof-shaped (case 5) and trapezoid-shaped roof (case 6) while, the TKE for upwind wedge-shaped roof (case 2) is observed to be lower than that at the other roof shapes.

In general, the previous results give evidence that the roofs shape configuration has a significant impact on the distribution of the turbulent kinetic energy inside an urban street canyon, especially when the wedge-shaped roof is placed on the upwind building of a canyon.

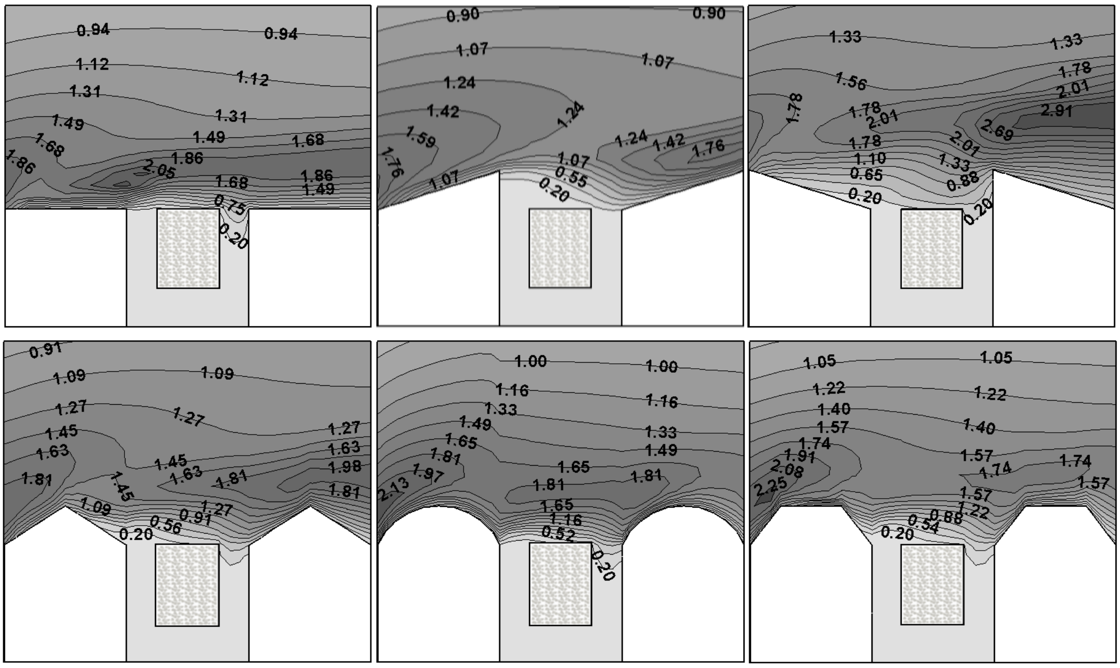

Fig. 7 Distribution of the turbulent kinetic energy at the mid-plane *y/H*=0, inside the urban street canyons for six different roof configurations

3.3 Pollutant dispersion

The dimensionless pollutant concentration (C^+) contours at the mid-plane (*y/H*= 0) inside the urban street canyons for six different roof configurations are shown in Fig. 8. In cases 1, 3, 4, 5 and 6 a large clockwise vortex circulation is observed within the street canyon. Consequently, the pollutant emitted by the lines sources is accumulated on the wall A side of the street canyon, and decreased from the floor to the roof of the upwind building, which extends upwards from the roof of the building. However, the pollutant concentration on the wall B side is lower than at the wall A side, and it's due to the recirculating flow between the buildings. The maximum concentration is found at the lower upwind building corner and the street floor. This indicates very poor ventilation properties due to the very small velocity distribution.

In case 2, the pollutant concentration at the floor and on leeward side is higher, and decreases in the vertical direction (from the floor to the upper region of the street), because the velocity is lower at the ground level of the street canyon and higher at the windward side.

By comparison between different cases, we can see that the pollution level in case 2 is also much higher than that for the other cases. While, the lower pollution level is observed in the case 5. In fact, the pollution level in street canyon changes with the change roof shapes of buildings.

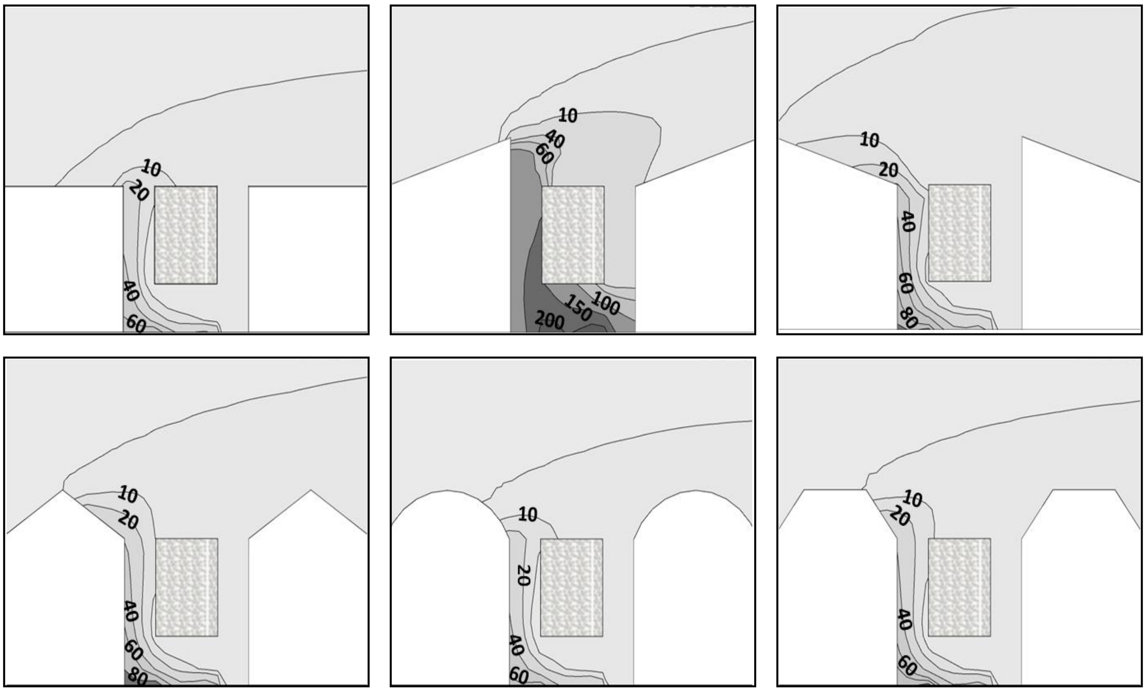

Fig. 8 Dimensionless pollutant concentration C^+ contours at the mid-plane *y*/*H*=0, inside the urban street canyons for six different roof configurations

Fig. 9 shows normalized pollutant concentration C+ on wall A and wall B for six different roof configurations. It can be seen clearly that the concentration level decreases from the centre to the street ends at both walls (A and B) for all cases. The average pollutant concentration at wall A is higher than at wall B about 12 times for case 1, 2 times for case 2, 39 times for case 3, 19 times for case 4, 14 times for case 5 and 17 times for case 6. Among the six cases studied in this work, the largest averaged pollutant concentration for two walls A and B is observed in case 2, while the smallest averaged pollutant concentration is observed in cases 1 and 5.

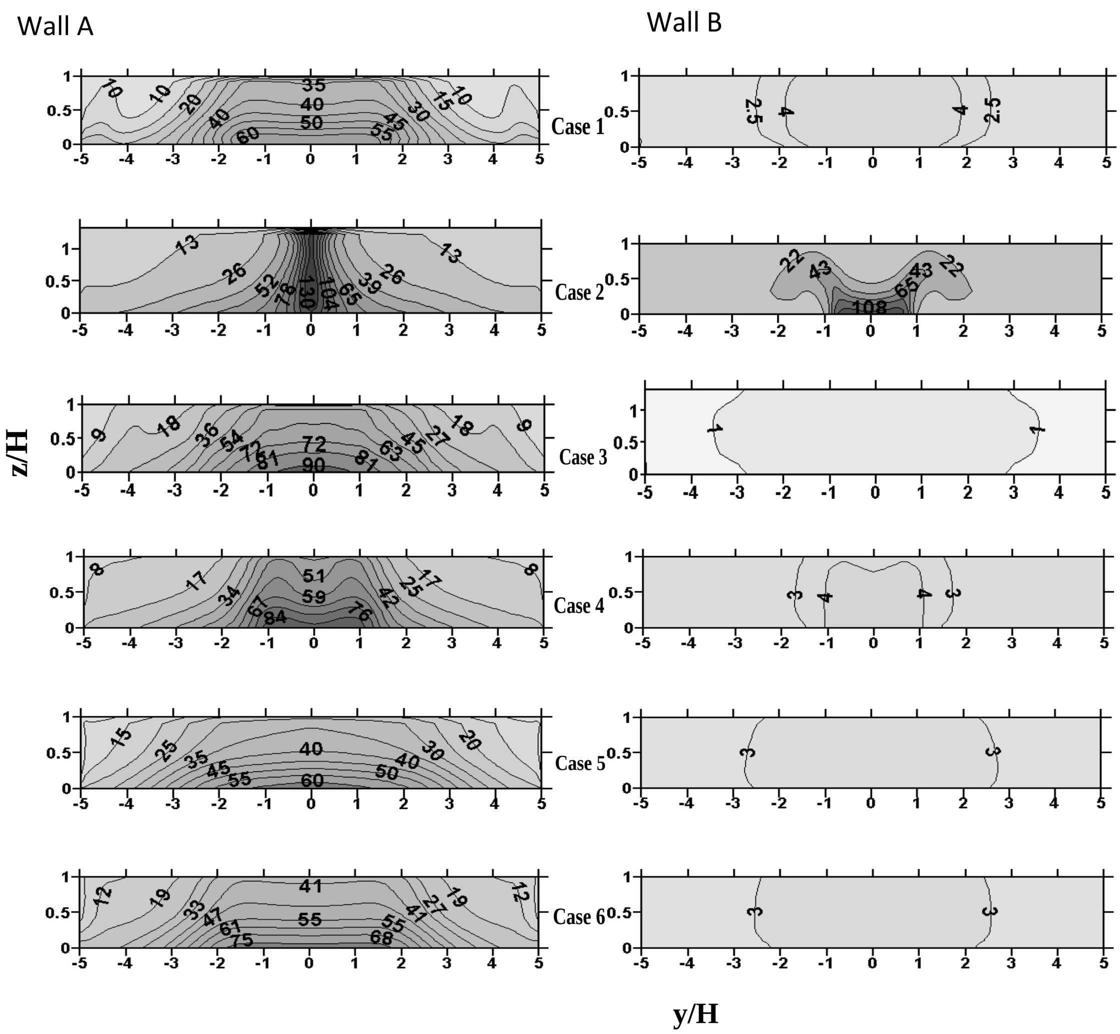

Fig. 9 Normalized concentration on Wall A (leeward) and Wall B (windward) for six different roof configurations

4. Conclusions

A three-dimensional computational fluid dynamics (CFD) model with the EARSM based *k-ε* turbulence model was used to simulate the fluid-flow development and pollutant dispersion in urban street canyons with tree planting of aspect ratio *W/H*=1 using ANSYS-CFX code. The numerical model was validated using the results of the wind tunnel experiments carried out at the University of Karlsruhe, Germany, and assessable to the scientific community from the online database (2008) <www.codasc.de>. Having established this, the influence of the roof building on airflow and pollutant dispersion in the street canyon with trees is investigated numerically.

The vortex configuration is different for the different roof shapes. The computed air velocity streamlines fields in street canyon with flat roof-shaped show that two fundamental vortex structures can be formed. These are clockwise canyon vortex inside the street canyons between the buildings, and the secondary vortex (corner eddies) located at the two ends of the street canyon. The in-canyon vortex dynamics (e.g., vortex orientation) are strongly dependent on the configuration of roof shape.

Because of flow separation as wind passes through the roofs peak (e.g., upwind and downwind wedge-shaped roof), both heights of upstream and downstream corners of the upwind and downwind building have a significant influence on the in-canyon vertical flow pattern.

The highest values of the TKE are found in the upper region toward the upwind building roof. The dissipation rate of TKE is different for each canyon depending on the roof shapes.

The pollutant concentration on the leeward walls is higher than that on the windward walls in the lower region for all cases. The corner eddies (at the two ends of the street canyon) provide additional ventilation and lead to lower traffic pollutant concentrations at the street canyon ends. At the mid-plane (*y/H*=0) inside the urban street canyons, the pollution level for the upwind wedge roof-shaped is much higher than that for the other cases. While, the lower pollution level is observed with the dome roof-shaped. The average pollutant concentration at leeward walls is higher than at windward walls by about 2.8 times for the flat roof-shaped, 6 times for the upwind wedge roof-shaped, 2.9 times for the downwind wedge roof-shaped, 19 times for slanted roof-shaped, 5.8 times for the dome roof-shaped and 6.9 times for the trapezoid roof-shaped. Among the six cases studied in this work, the largest pollutant concentration level for two walls of the street canyon (leeward and windward walls) is observed with the upwind wedge-shaped roof. The smallest pollutant concentration level is observed with the dome roof-shaped.

This work will be important and useful for architects to choose the most optimum shaped configurations of building roof, which reduces adverse impact on local air quality in street canyons with trees planting.

References

Ahmadi, G. and Li, A. (2000), "Computer simulation of particle transport and deposition near a small isolated building", *J. Wind Eng. Ind. Aerod.*, **84**(1), 23-46.

ANSYS CFX-Solver Theory Guide (2013).

Baik, J.J. and Kim, J.J. (1999), "A numerical study of flow and pollutant dispersion characteristics in urban street canyons", *J. Appl. Meteorol.*, **38**, 1576-1589.

Becker, S., Lienhart, H. and Durst, F. (2002), "Flow around three-dimensional obstacles in boundary layers", *J. Wind Eng. Ind. Aerod.*, **90**(4-5), 265-279.

Buccolieri, R., Gromke, C., Di Sabatino, S. and Ruck, B. (2009), "Aerodynamic effects of trees on pollutant concentration in street canyons", *Sci. Total Environ.*, **407**(19), 5247-5256.

Buccolieri, R., Salim, S.M., Leo, L.S., Di Sabatino, S., Chan, A. and Ielpo, P. (2011), "Analysis of local scale tree-atmosphere interaction on pollutant concentration in idealized street canyons and application to a real urban junction", *Atmos. Environ.*, **45**(9), 1702-1713.

Cai, X.M., Barlow, J.F. and Belcher, S.E. (2008), "Dispercsion and transfer of passive scalar sin and above street canyons —large-eddy simulations", *Atmos. Environ*., **42**(23), 5885-5895.

Chan, T.L., Dong, G., Leung, C.W., Cheung, C.S. and Hung, W.T. (2002), "Validation of a two- dimensional pollutant dispersion model in an isolated street canyon", *Atmos. Environ.*, **36**(5), 861-872.

Chang ,C. and Meroney, R.N. (2003), "Concentration and flow distributions in urban street canyons: wind tunnel and computational data", *J. Wind Eng. Ind. Aerod.*, **91**(9), 1141-1154.

CODASC (Concentration Data of Street Canyons). (2008), Laboratory of Building- and Environmental Aerodynamics, IfH, Karlsruhe Institute of Technology.

Di Sabatino, S., Buccolieri, R., Pulvirenti, B. and Britter, R. (2008), "Flow and pollutant dispersion in street canyons using FLUENT and ADMS-Urban", *Environ. Model. Assessment*, **13**(3), 369-381.

Eliasson, I., Offerle, B., Grimmond, C.S.B. and Lindqvist, S. (2006), "Wind fields and turbulence statistics in an urban street canyon", *Atmos. Environ.*, **40**(1), 1-16.

Gerdes, F. and Olivarin, D. (1999), "Analysis of pollutant dispersion in an urban street canyon", *J. Wind Eng. Ind. Aerod.*, **82**(1-3), 105-124.

Gromke, C. and Blocken, B. (2015a), "Influence of avenue-trees on air quality at the urban neighborhood scale. Part I: Quality assurance studies and turbulent Schmidt number analysis for RANS CFD simulations", *Atmos. Environ.*, **196**, 214-223.

Gromke, C. and Blocken, B. (2015b), "Influence of avenue-trees on air quality at the urban neighborhood scale. Part II: Traffic pollutant concentrations at pedestrian level", *Atmos. Environ.*, **196**, 214-223.

Gromke, C. and Ruck, B. (2007), "Influence of trees on the dispersion of pollutant in an urban street canyon—experimental investigation of the flow and concentration field", *Atmos. Environ.*, **41**(16), 3287-3302.

Gromke, C. and Ruck, B. (2009), "On the impact of trees on dispersion processes of traffic emissions in street canyons", *Bound. – Lay. Meteorol.*, **131**(1), 19-34.

Gromke, C. and Ruck, B. (2012), **"**Pollutant concentrations in street canyons of different aspect ratio with avenues of trees for various wind directions", *Bound. – Lay. Meteorol.*, **144**(1), 41-64.

Gromke, C., Buccolieri, R., Di Sabatino, S. and Ruck, B. (2008), "Dispersion study in a street canyon with tree planting by means of wind tunnel and numerical investigations—evaluation of CFD data with experimental data", *Atmos. Environ.*, **42**(37), 8640-8650.

Hanna, S.R., Tehranian, S., Carissimo, B., Macdonald, R.W. and Lohner, R. (2002), "Comparisons of model simulations with observations of mean flow and turbulence within simple obstacle arrays", *Atmos. Environ.*, **36**(32), 5067-5079.

Huang, Y., Hu, X. and Zeng, N. (2009), "Impact of wedge-shaped roofs on airflow and pollutant dispersion inside urban street canyons", *Build. Environ.*, **44** (12), 2335-2347.

Hunter, L.J., Johnson, G.T. and Watson, I.D. (1992), "An investigation of three-dimensional characteristics of flow regimes within the urban canyon", *Atmos. Environ.*, **26**(4), 425-432.

Kastner-Klein, P. and Plate, E.J. (1999), "Wind-tunnel study of concentration fields in street canyons", *Atmos. Environ.*, **33**(24-25), 3973-3979.

Kastner-Klein, P., Fedorovich, E. and Rotach, M.W. (2001), "A wind tunnel study of organised and turbulent air motions in urban street canyons ", *J. Wind Eng. Ind. Aerod.*, **89**(9), 849-861.

Kim, J.J. and Baik, J.J. (2003), "Effects of inflow turbulence intensity on flow and pollutant dispersion in an urban street canyon ", *J. Wind Eng. Ind. Aerod.*, **91**(3), 309-329.

Meroney, N.R., Leitl, B.M., Rafailidis, S. and Schatzmann, M. (1999), "Wind-tunnel and numerical modeling of flow and dispersion about several building shapes", *J. Wind Eng. Ind. Aerod.*, **81**(1-3), 333-345.

Meroney, R.N. (1982), "Turbulent diffusion near buildings. (Ed., E.J. Plate)", *Engineering Meteorology*, Elsevier, Amsterdam,. 425-481.

Meroney, R.N., Pavageau, M., Rafadalis, S. and Schatzmann, M. (1996), "Study of line source characteristics for 2D physical modelling of pollutant dispersion in street canyons", *J. Wind Eng. Ind. Aerod.*, **62**(1), 37-56.

Moonen, P., Gromke, C. and Dorer, V. (2013), **"**Performance assessment of large eddy simulation (LES) for modelling dispersion in an urban street canyon with tree planting", *Atmos. Environ.*, ***75***, 66-76.

Nazridoust, K. and Ahmadi, G. (2006), "Airflow and pollutant transport in street canyons", *J. Wind Eng. Ind. Aerod.*, **94**(6), 491-522.

Pavageau, M. and Schatzmann, M. (1999), "Wind tunnel measurements of concentration fluctuations in an urban street canyon", *Atmos. Environ.*, **33**(24-25), 3961-3971.

Sahm, P., Louka, P., Ketzel, M., Guillouteau, E. and Sini, J.F. (2002), "Intercomparison of numerical urban dispersion models. Part I: Street canyon and single building configurations", *Water Air Soil Pollution Focus*, **2**(5), 587-601.

Salim, M.S., Riccardo, B., Andrew, C. and Silvana, D.S. (2011), "Numerical simulation of atmospheric pollutant dispersion in an urban street canyon: Comparison between RANS and LES", *J. Wind Eng. Ind. Aerod.*, **89**(2-3), 849-861.

Santiago, J.L. and Martín, F. (2008), "SLP-2D: a new Lagrangian particle model to simulate pollutant dispersion in street canyons", *Atmos. Environ.*, **42**(17), 3927-3936.

Sini, J.F., Anquetin, S. and Mestayer, G. (1996), "Pollutant dispersion and thermal effects in urban street canyons", *Atmos. Enviro.*, **30**(15), 2659-2677.

Wallin, S. and Johansson, A. (2000), **"**A complete explicit algebraic Reynolds stress model for incompressible and compressible flows", *J. Fluid Mech.*, **403**, 89-132.

Xie, X.M., Huang, Z. and Wang, J.S. (2005), "Impact of building configuration on air quality in street canyon", *Atmos. Environ.*, **39**(25), 4519-4530.

CC